[CANCER RESEARCH 61, 1781–1785, March 1, 2001]

Advances in Brief

Noninvasive Imaging of $\alpha_v\beta_3$ Integrin Expression Using ^{18}F-labeled RGD-containing Glycopeptide and Positron Emission Tomography[1]

Roland Haubner,[2] Hans-Jürgen Wester, Wolfgang A. Weber, Christian Mang, Sibylle I. Ziegler, Simon L. Goodman, Reingard Senekowitsch-Schmidtke, Horst Kessler, and Markus Schwaiger

Department of Nuclear Medicine, Technische Universität München, 81675 München, Germany [R. H., H-J. W., W. A. W., S. I. Z., R. S-S., M. S.]; Institute of Organic Chemistry and Biochemistry, Technische Universität München, 85747 Garching, Germany [C. M., H. K.]; and Department of Preclinical Oncology, Merck KGaA, 64271 Darmstadt, Germany [S. L. G.]

Abstract

The $\alpha_v\beta_3$ integrin is an important cell adhesion receptor involved in tumor-induced angiogenesis and tumor metastasis. Here we describe the ^{18}F-labeling of the RGD-containing glycopeptide cyclo(-Arg-Gly-Asp-D-Phe-Lys(sugar amino acid)-) with 4-nitrophenyl 2-[^{18}F]fluoropropionate and the evaluation of this compound *in vitro* and in tumor mouse models. Binding assays with isolated immobilized $\alpha_v\beta_3$, $\alpha_v\beta_5$, and $\alpha_{IIb}\beta_3$ as well as *in vivo* studies using $\alpha_v\beta_3$-positive and -negative murine and xenotransplanted human tumors demonstrated receptor-specific binding of the radiolabeled glycopeptide yielding high tumor:background ratios (*e.g.*, 120 min postinjection: tumor:blood, 27.5; tumor:muscle, 10.2). First imaging results using a small animal positron emission tomograph suggest that this compound is suitable for noninvasive determination of the $\alpha_v\beta_3$ integrin status and therapy monitoring.

Introduction

Numerous studies have shown that the integrin $\alpha_v\beta_3$ is an important receptor affecting tumor growth, local invasiveness, and metastatic potential (1). This dimeric transmembrane glycoprotein mediates adhesion and migration of tumor cells on a variety of extracellular matrix proteins. Furthermore, $\alpha_v\beta_3$ is strongly expressed on activated endothelial cells and plays a critical role in the angiogenic process (2). In contrast, expression of $\alpha_v\beta_3$ is weak in resting endothelial cells and most normal organ systems. Thus, inhibition of $\alpha_v\beta_3$ is currently being evaluated as a new strategy for tumor-specific anticancer therapy. Similar to several other integrins, $\alpha_v\beta_3$ recognizes the tripeptide sequence arginine-glycine-aspartic acid (RGD). The affinity of integrins toward different ligands is critically determined by the conformation of this common binding motif. Thus, the design of RGD-containing peptides with the corresponding conformation allows selective targeting of specific integrins. In previous studies (3, 4), we used spatial screening techniques for the development of the first α_v-selective inhibitor, cyclo(-Arg-Gly-Asp-D-Phe-Val-) (5). More recently, peptidomimetic $\alpha_v\beta_3$ antagonists have been developed (6, 7). Inhibition of $\alpha_v\beta_3$ function by these peptidic and nonpeptidic antagonists has been shown to inhibit tumor growth in animal studies (6–8). Future developments of anti-$\alpha_v\beta_3$-directed therapy and translation of these encouraging experimental data to clinical studies would be greatly facilitated by noninvasive techniques that allow serial studies of $\alpha_v\beta_3$-positive tumors. In an animal model, Sipkins *et al.* (9) recently demonstrated that it is feasible to image $\alpha_v\beta_3$ expression using magnetic resonance imaging and antibody-coated paramagnetic liposomes.

The aim of this study was to develop a radiolabeled analogue of cyclo(-Arg-Gly-Asp-D-Phe-Val-) that is suitable for imaging of $\alpha_v\beta_3$ expression using PET.[3] In addition, the feasibility of small animal PET systems for monitoring blockade of $\alpha_v\beta_3$ by specific antagonists was evaluated in living mice.

Materials and Methods

All organic reagents were purchased from Merck KGaA (Darmstadt, Germany), Aldrich (Steinheim, Germany), or Fluka (Neu-Ulm, Germany) and used without further purification. Human M21 and M21-L melanoma cells were kindly provided by Dr. D. A. Cheresh (Departments of Immunology and Vascular Biology, The Scripps Research Institute, La Jolla, CA). Analytical as well as preparative RP-HPLC was performed on Sykam equipment (Gilching, Germany) using a YMC-Pack J'sphere H80 (4 μm; 150 $\times$ 20 mm) column (YMC Co., Ltd., Kyoto, Japan). For radioactivity measurements, the outlet of the UV detector was connected to a well-type NaI(Tl) detector from EG&G (München, Germany).

Preparation of [^{18}F]Galacto-RGD. The synthesis of the Fmoc-protected SAA (7-amino-L-glycero-L-galacto-2,6-anhydro-7-deoxyheptanoic acid) and the fluorination precursor [cyclo(-Arg-Gly-Asp-D-Phe-Lys(SAA)-)] as well as the reference glycopeptide will be described elsewhere.[4] N.c.a. [^{18}F]fluoride ($t_{1/2}$ =109.7 min) was produced via the ^{18}O(p,n)^{18}F nuclear reaction by bombardment of an isotopically enriched [^{18}O]water target with an 11 MeV proton beam using the RDS-112 cyclotron (Siemens/CTI, Knoxville, TN). The glycopeptide was labeled using n.c.a. 4-nitrophenyl 2-[^{18}F]fluoropropionate (specific activity, approximately 70 TBq/mmol), which was prepared as described by Wester *et al.* (10). Briefly, 6 μmol of cyclo(-Arg-Gly-Asp-D-Phe-Lys(SAA)-) were dissolved in 150 μl of DMSO and added to an Eppendorf cap with dried 4-nitrophenyl 2-[^{18}F]fluoropropionate (approximately 185 MBq). After this, 30 μmol of potassium salt of 1-hydroxy-benzotriazole in 50 μl of DMSO were added and allowed to stand for 15 min at 70°C. Isolation of the ^{18}F-labeled glycopeptide was carried out using RP-HPLC with an acetonitrile/water/0.1% trifluoroacetic acid gradient (10–50% acetonitrile in 20 min; flow rate, 10 ml/min, t_R = 11.6 min, K' = 5.1). The solvent was removed *in vacuo*, and the residue was dissolved in PBS (pH 7.4) to obtain solutions that were ready for use in animal experiments.

Biological Assay. Purification of the proteins and the isolated integrin binding assay have been described elsewhere (11). The inhibitory capacities of [^{19}F]Galacto-RGD were quantified by measuring its effect on the interactions between immobilized integrin and biotinylated soluble ligands (vitronectin or fibrinogen). The integrin preparations differ somewhat over time, thus the α_v-selective cyclo(-Arg-Gly-Asp-D-Phe-Val-) was used as internal standard to allow interassay comparability.

Received 8/7/00; accepted 1/12/01.

The costs of publication of this article were defrayed in part by the payment of page charges. This article must therefore be hereby marked *advertisement* in accordance with 18 U.S.C. Section 1734 solely to indicate this fact.

[1] Supported by Grant 96.017.2 from the Sander-Foundation and in part by the German Reseach Foundation.

[2] To whom requests for reprints should be addressed, at Department of Nuclear Medicine, Klinikum rechts der Isar, Technische Universität München, Ismaninger Strasse 22, D-81675 München, Germany. Phone: 49-89-41404554; Fax: 49-89-41404841; E-mail: R.Haubner@lrz.tum.de.

[3] The abbreviations used are: PET, positron emission tomography; RP-HPLC, reversed-phase high performance liquid chromatography; SAA, sugar amino acid; Fprop, 2-fluoropropionyl; [^{18}F]Galacto-RGD, cyclo(-Arg-Gly-Asp-D-Phe-Lys(([^{18}F]Fprop)SAA)-); p.i., postinjection; %ID/g, percentage of the injected dose per gram of tissue; n.c.a., non-carrier added.

[4] R. Haubner, H. J. Wester, C. Mang, S. L. Goodman, H. Kessler, and M. Schwaiger. Synthesis and *in vitro* evaluation of a RGD-containing glycopeptide for the noninvasive determination of the $\alpha_v\beta_3$ expression using PET, manuscript in preparation.

Tumor Models. Biodistribution of [^{18}F]Galacto-RGD was evaluated in mice using a murine osteosarcoma and two xenotransplanted human melanoma models (M21 and M21-L). The osteosarcoma and the M21 melanoma cell line both express the $\alpha_v\beta_3$ integrin (11, 12). The melanoma M21-L cell line, which was selected for weak expression of the $\alpha_v\beta_3$ integrin, served as a negative control (12).

Murine osteosarcomas induced by injection of strontium-90 were serially transplanted into female BALB/c mice. Tumor pieces of approximately 1 mm^3 were injected by a trocar close to the femur into the musculus quadriceps. Human M21 and M21-L melanoma cells were cultured in a humidified atmosphere with 5% CO_2. The cell culture medium was RPMI 1640 (Seromed Biochrom, Berlin, Germany) supplemented with 10% FCS and gentamicin. Tumor xenografts were obtained by s.c. injection of 5×10^6 cells (M21) or 1.5×10^7 cells (M21-L) into the left flank of female nude mice. Mice bearing tumors weighing between 300 and 500 mg were used for biodistribution studies.

Biodistribution Studies. Nude mice bearing tumor xenografts of human melanoma M21 or M21-L and BALB/c mice bearing murine osteosarcomas were i.v. injected with approximately 370 kBq of [^{18}F]Galacto-RGD. The animals were sacrificed and dissected 10, 60, and 120 min after injection of [^{18}F]Galacto-RGD. Blood, plasma, liver, kidney, muscle, heart, brain, lung, spleen, colon, femur, and tumor were removed and weighed. The radioactivity in the tissue was measured using a gamma counter. Results are expressed as the %ID/g. Each value represents the mean and SD of three to four animals.

Competition Studies. Blocking of the $\alpha_v\beta_3$ integrin was completed by injecting 6 mg/kg cyclo(-Arg-Gly-Asp-D-Phe-Val-) 10 min before the injection of 370 kBq of the radioactive compound in 100 μl of PBS (pH 7.4). Animals were sacrificed and dissected 60 min after injection of [^{18}F]Galacto-RGD. Further processing was carried out as described above.

PET Studies with a Dedicated Small Animal Scanner. PET imaging of tumor-bearing mice was performed using a prototype small animal positron tomograph, Munich Avalanche Photodiode PET (13). The animal scanner consists of two sectors, comprising three detector modules each, which rotate around the animal for acquisition of complete projections in one transaxial slice (30 angular steps). Each module consists of eight small ($3.7 \times 3.7 \times 12$ mm^3) lutetium-oxy-orthosilicate crystals read out by arrays of avalanche photodiodes. List mode data are reconstructed using statistical, iterative methods including the spatially dependent line spread function. Reconstructed image resolution is 2.5 mm (full width at half maximum) in a transaxial field of view of 7.5 cm, and the slice thickness is 2 mm. Ninety min after the injection of approximately 5.5 MBq of [^{18}F]Galacto-RGD, animals were positioned prone inside the tomograph, and a transaxial slice through the tumor region was measured for 35 min.

One melanoma M21-bearing mouse was imaged three times: (*a*) without pretreatment; (*b*) with 6 mg/kg cyclo(-Arg-Gly-Asp-d-Phe-Val-); and (*c*) with 18 mg/kg cyclo(-Arg-Gly-Asp-d-Phe-Val-) injected 10 min before the tracer. For comparison, one mouse with negative control melanoma M21-L was imaged. Tumor volume was approximately 0.5 ml for both tumor models. To assess tumor uptake of [^{18}F]Galacto-RGD, circular regions of interest with a diameter of 5 mm were placed at the location of the maximum tracer uptake in the tumor and in the contralateral thorax wall (reference region). Relative tracer uptake was expressed as the ratio between mean counts in the tumor and in the reference region (tumor:background ratio).

Results

Labeling of cyclo(-Arg-Gly-Asp-D-Phe-Lys(SAA)-) using 4-nitrophenyl 2-[^{18}F]fluoropropionate as a prosthetic group resulted in [^{18}F]Galacto-RGD (Fig. 1) of high radiochemical purity (>98%). The decay-corrected radiochemical yield for the acylation step after RP-HPLC was approximately 50% within a total preparation time of about 40 min.

The *in vitro* binding assay showed that the inhibitory peptides were able to fully suppress the binding of the ligands (vitronectin or fibrinogen) to the isolated immobilized receptors ($\alpha_{IIb}\beta_3$, $\alpha_v\beta_5$, and $\alpha_v\beta_3$) and that the binding kinetics followed a classic sigmoid path. The IC_{50}s of [^{18}F]Galacto-RGD were 5 ($\alpha_v\beta_3$), 1.000 ($\alpha_v\beta_5$), and 6.000 nM ($\alpha_{IIb}\beta_3$), respectively. Thus, [^{18}F]Galacto-RGD showed a 200-1200-fold higher affinity for $\alpha_v\beta_3$ than for $\alpha_v\beta_5$ and $\alpha_{IIb}\beta_3$, respectively.

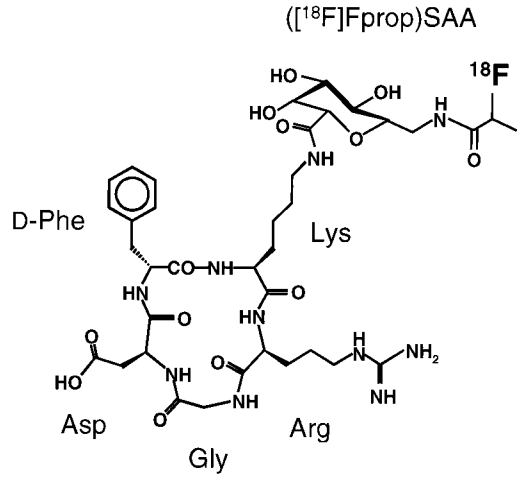

Fig. 1. Schematic structure of [^{18}F]Galacto-RGD. The glycopeptide shows the characteristic βII'-turn with D-Phe in the i+1 position and the RGD site in a "kinked" conformation responsible for the $\alpha_v\beta_3$ selectivity.

The biodistribution data of [^{18}F]Galacto-RGD in the three tumor models are summarized in Table 1. [^{18}F]Galacto-RGD showed rapid and predominantly renal excretion, resulting in a low activity concentration in blood and muscle as early as 60 min p.i. The initial activity accumulation in the $\alpha_v\beta_3$-expressing osteosarcoma and melanoma M21 was between 3% and 4% ID/g 10 min p.i., decreasing to about 1.5% ID/g 60 min p.i. and remaining constant until the end of the observation period. Moreover, at 120 min p.i., most organs showed lower activity uptake like the tumor for both models. Only liver, colon, and kidneys revealed a similar activity concentration to the tumor. The low activity accumulation in the bone indicated that the tracer is stable toward defluorination *in vivo*. Altogether, this led to high tumor:background ratios [*e.g.*, tumor:blood, 13.2 (osteosarcoma) and 27.5 (M21); tumor:muscle: 6.0 (osteosarcoma) and 10.2 (M21)]. In contrast, the negative control tumors showed an initial tracer uptake of approximately 2% ID/g, which decreased to about 0.4% ID/g after 60 min p.i. Thus, the tracer uptake in the negative control tumor is 3.8 times lower than that in the $\alpha_v\beta_3$-positive tumor between 60 and 120 min (Fig. 2). Pretreatment of the melanoma M21-bearing mice with 6 mg/kg of the α_v-selective peptide cyclo(-Arg-Gly-Asp-D-Phe-Val-) reduced the tumor:blood ratio at 60 min p.i. from 8.7 to 1.5 and the tumor:muscle ratio from 7.4 to 4.2.

The transaxial image (Fig. 3) of a melanoma M21-bearing mouse obtained by the animal scanner demonstrates the high tumor:background ratio found in the biodistribution studies and allowed clear visualization of the $\alpha_v\beta_3$-expressing tumor in the left flank of the mouse. In contrast, the same experiment using a mouse with the negative control melanoma M21-L on the left flank showed almost no increased activity uptake in the tumor compared to the background (tumor:background, 1.2). Moreover, pretreatment experiments with different amounts of cyclo(-Arg-Gly-Asp-D-Phe-Val-) injected 10 min before the tracer demonstrated dose-dependent blocking of the $\alpha_v\beta_3$ integrin (Fig. 3). The tumor:background ratio decreased from 5.7 (without pretreatment) to 3.2 [pretreatment with 6 mg/kg cyclo(-Arg-Gly-Asp-D-Phe-Val-)] and 2.1 [pretreatment with 18 mg/kg cyclo(-Arg-Gly-Asp-D-Phe-Val-)].

Discussion

In this study, we described the first ^{18}F-labeled RGD-containing glycopeptide ([^{18}F]Galacto-RGD) that is suitable for noninvasive

Table 1 *Biodistribution data for [^{18}F]Galacto-RGD in melanoma-bearing nude mice and osteosarcoma-bearing mice*

Values are given as % ID/g ± SD.

Time p.i. (min)	Osteosarcoma ($\alpha_v\beta_3$ positive)	Melanoma M21 ($\alpha_v\beta_3$ positive)	Melanoma M21-L (negative control)
Blood			
10	2.58 ± 0.41	2.93 ± 0.53	4.70[a]
60	0.27 ± 0.06	0.18 ± 0.06	0.26 ± 0.06
120	0.13 ± 0.03	0.05 ± 0.01	0.13 ± 0.07
Serum			
10	5.25 ± 0.33	5.65 ± 0.89	8.71
60	0.50 ± 0.12	0.34 ± 0.11	0.49 ± 0.11
120	0.19 ± 0.04	0.09 ± 0.01	0.22 ± 0.10
Liver			
10	5.47 ± 0.11	5.64 ± 2.27	6.40
60	2.94 ± 0.27	1.85 ± 0.39	2.07 ± 0.20
120	1.97 ± 0.27	1.25 ± 0.05	1.79 ± 0.58
Kidneys			
10	8.67 ± 0.52	8.48 ± 0.84	10.82
60	3.11 ± 0.60	1.86 ± 0.10	2.24 ± 0.21
120	2.21 ± 0.46	1.52 ± 0.10	1.86 ± 0.46
Muscle			
10	0.80 ± 0.13	1.13 ± 0.18	1.44
60	0.32 ± 0.06	0.21 ± 0.02	0.21 ± 0.03
120	0.28 ± 0.02	0.15 ± 0.02	0.18 ± 0.03
Spleen			
10	2.54 ± 0.07	2.10 ± 0.45	2.39
60	1.54 ± 0.22	0.69 ± 0.10	0.77 ± 0.02
120	1.20 ± 0.04	0.64 ± 0.09	0.73 ± 0.14
Heart			
10	1.94 ± 0.05	1.85 ± 0.24	2.02
60	0.51 ± 0.07	0.28 ± 0.05	0.34 ± 0.02
120	0.63 ± 0.41	0.19 ± 0.04	0.29 ± 0.06
Tumor			
10	2.88 ± 0.32	3.90 ± 1.36	1.88
60	1.33 ± 0.20	1.56 ± 0.15	0.42 ± 0.09
120	1.68 ± 0.49	1.49 ± 0.10	0.44 ± 0.24
Lung			
10	3.43 ± 0.24	3.64 ± 0.52	4.84
60	1.10 ± 0.18	0.76 ± 0.09	0.83 ± 0.08
120	0.72 ± 0.15	0.53 ± 0.05	0.71 ± 0.24
Femur			
10	1.22 ± 0.04	1.51 ± 0.34	1.46
60	0.54 ± 0.11	0.34 ± 0.05	0.44 ± 0.06
120	0.51 ± 0.02	0.33 ± 0.02	0.50 ± 0.10
Colon			
10	3.77 ± 0.16	1.74 ± 0.55	1.68
60	2.27 ± 1.23	0.57 ± 0.04	0.70 ± 0.19
120	1.59 ± 0.46	3.53 ± 0.44	0.76 ± 0.27
Brain			
10	0.14 ± 0.01	0.19 ± 0.04	0.19
60	0.06 ± 0.01	0.05 ± 0.01	0.05 ± 0.01
120	0.05 ± 0.01	0.04 ± 0.01	0.05 ± 0.01

[a] Data for this time point result from one mouse.

imaging of $\alpha_v\beta_3$ integrin expression using PET. Imaging of $\alpha_v\beta_3$-positive tumors in living mice using a high-resolution PET scanner resulted in a strong contrast between tumor and normal tissues. Moreover, we demonstrated that serial PET studies using [^{18}F]Galacto-RGD allowed noninvasive assessment of the blockade of the receptor by specific antagonists.

Previously, we introduced radioiodinated cyclic RGD peptides for the imaging of $\alpha_v\beta_3$ integrin status (11). These first-generation tracers showed receptor-specific accumulation in different tumor mouse models. However, these tracers also revealed high activity retention in liver and intestine, which limits the application for tumor imaging. For the present study, we improved the pharmacokinetics by introducing a SAA, which increased the hydrophilicity and markedly reduced the tracer uptake by the liver. Moreover, introduction of the SAA allows ^{18}F-labeling of the amino methyl function of the glycopeptide using radiolabeled acylation reagents. The design of [^{18}F]Galacto-RGD was based on our data from comprehensive structure activity investigations (3–5, 14). These studies demonstrated that the specific binding of the cyclic pentapeptides is determined by a "kinked" conformation of the RGD site (see Fig. 1). Introduction of a lysine and subsequent conjugation of the SAA are not expected to change the spatial structure of the peptide. Thus, these modifications are unlikely to influence the $\alpha_v\beta_3$ affinity of the compound. This was confirmed by the *in vitro* binding studies, which revealed a high $\alpha_v\beta_3$ affinity and selectivity for [^{18}F]Galacto-RGD.

Moreover, [^{18}F]Galacto-RGD showed rapid and predominantly renal excretion, resulting in a low tracer concentration in most of the organs (especially blood and muscle) and stable accumulation in the $\alpha_v\beta_3$-expressing tumor during the observation period (up to 120 min p.i.). These features permit high signal:noise ratios for *in vivo* imaging soon after injection (2 h), making this tracer suitable for PET studies using short-lived isotopes.

Recently, different nonpeptidic antagonists with high affinity and selectivity have been reported (6, 7). These low molecular mass compounds are optimized in size to fit the binding pocket of the receptor. Thus, introduction of labeling groups is likely to result in a loss of affinity. Sivolapenko *et al.* (15) described a ^{99m}Tc-labeled linear decapeptide containing two RGD sites that had been used for imaging in one patient study. However, neither *in vitro* nor *in vivo* studies were carried out to demonstrate $\alpha_v\beta_3$ affinity and specificity of the peptide. Furthermore, the linear peptide showed high persistent background activity in the lung and abdomen. Most recently, preliminary data have been presented on a ^{111}In-labeled diethylenetriamine-penta-acetic acid-RGD analogue (16), a dimeric, 12-amino acid $\alpha_v\beta_3$ antagonist labeled with ^{99m}Tc or ^{111}In (17), and ^{99m}Tc-, ^{186}Re-, and ^{90}Y-labeled peptides based on cyclo(-Arg-Gly-Asp-D-Phe-Lys-) (18). These compounds showed tumor-specific binding *in vitro* and *in vivo*.

However, the use of a PET tracer is preferable for imaging receptor

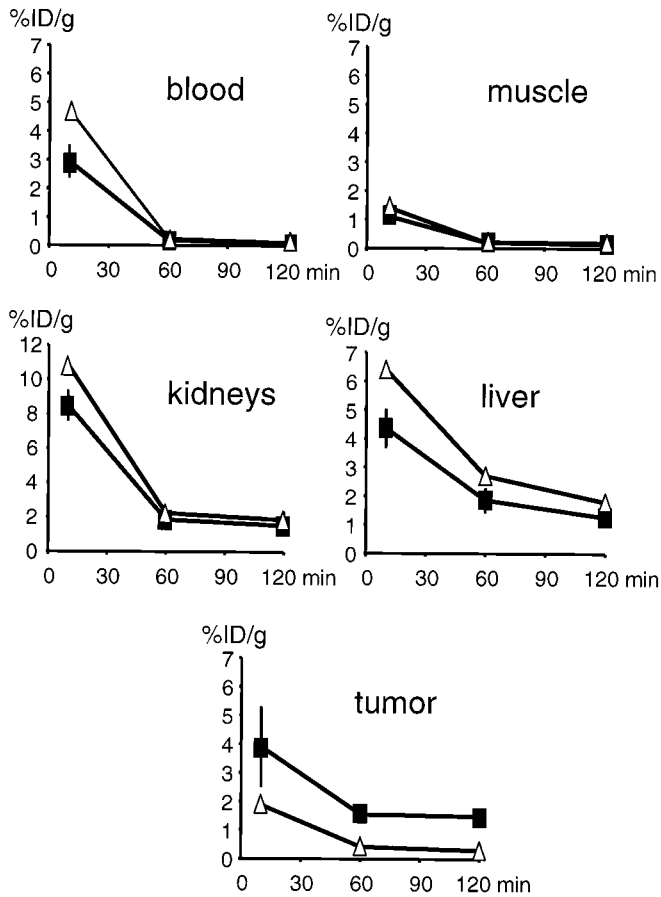

Fig. 2. Comparison of the biodistribution data of [^{18}F]Galacto-RGD in melanoma M21 (■)- and M21-L (△)-bearing nude mice. *Error bars*, 1 SD. For some data points, error bars are not visible because the SD is smaller than the size of the symbol.

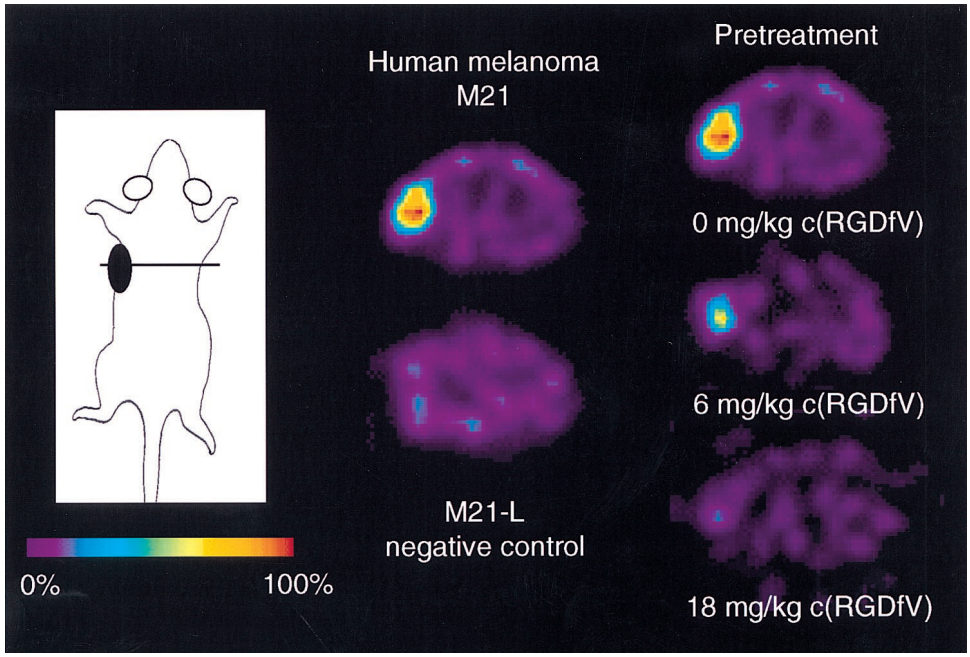

Fig. 3. Transaxial small animal PET images of nude mice bearing human melanoma xenografts. Images were acquired 90 min after injection of approximately 5.5 MBq of [^{18}F]Galacto-RGD. The *top left* image shows selective accumulation of the tracer in the $\alpha_v\beta_3$-positve (M21) tumor on the left flank. In contrast, no focal tracer accumulation is visible in the $\alpha_v\beta_3$-negative (*M21-L*) control tumor (*bottom left image*). The three images on the *right* were obtained from serial [^{18}F]Galacto-RGD PET studies in one mouse. These illustrate the dose-dependent blockade of tracer uptake by the α_v-selective cyclic pentapeptide cyclo(-Arg-Gly-Asp-D-Phe-Val-).

expression because of the superior sensitivity and spatial resolution of PET and the ability to quantify regional tracer concentrations. As demonstrated by our study, these principal physical advantages of PET permit imaging of $\alpha_v\beta_3$ expression in living mice. Furthermore, we were able to demonstrate the feasibility of serial PET studies to determine the specific blockade of $\alpha_v\beta_3$ after injection of increasing amounts of cyclo(-Arg-Gly-Asp-D-Phe-Val-), a potent α_v antagonist. This indicates that [^{18}F]Galacto-RGD may also be used for monitoring anticancer therapy directed at the functional inhibition of $\alpha_v\beta_3$.

Although these data are very encouraging, the following limitations should also be noted. In this initial evaluation of [^{18}F]Galacto-RGD, $\alpha_v\beta_3$ receptor density was not quantitatively determined for the tumor models. Furthermore, PET studies were analyzed by simple tumor: background ratios. Quantitative analysis of $\alpha_v\beta_3$ receptor density by PET imaging will require tracer kinetic analysis and correlation with the expression of the $\alpha_v\beta_3$ integrin using immunohistochemistry and Western blots. Nevertheless, the uptake of [^{18}F]Galacto-RGD in $\alpha_v\beta_3$-positive tumors was four times higher than that in negative controls, and a specific antagonist was able to block up to 65% of [^{18}F]Galacto-RGD uptake in receptor-positive tumors. Moreover, as reported previously (11), the nonspecific radiolabeled cyclic pentapeptide 3-[^{125}I]iodo-Tyr^4-cyclo(-Arg-D-Ala-Asp-Tyr-Val-) clearly showed lower tumor uptake for both tumor models (osteosarcoma, 0.48 ± 0.39% ID/g at 120 min p.i.; melanoma M21, 0.12 ± 0.04% ID/g at 120 min p.i.). Thus, our findings qualitatively demonstrate receptor specificity of [^{18}F]Galacto-RGD *in vivo*. In addition, the good correlation between tumor:background ratios determined by small animal PET and invasive biodistribution studies clearly indicate the feasibility of quantitative evaluation of $\alpha_v\beta_3$ expression by PET imaging.

The use of n.c.a. [^{18}F]Galacto-RGD in humans is not expected to lead to toxicity because plasma concentrations will be in the low nanomolar range. Furthermore, the short physical half-life of ^{18}F ($t_{1/2}$ = 109.7 min) and rapid renal elimination of unbound tracer result in a low radiation dose. Thus, PET studies using [^{18}F]Galacto-RGD may easily be translated from experimental settings to clinical studies.

Initial clinical trials evaluating the use of $\alpha_v\beta_3$ antagonists as antiangiogenic therapy in patients with various malignant tumors have been initiated (19). In clinical studies, radiolabeled RGD peptides may be used to document $\alpha_v\beta_3$ expression of the tumors before the administration of $\alpha_v\beta_3$ antagonists, thus allowing appropriate selection of patients entering clinical trials. Furthermore, as demonstrated, [^{18}F]Galacto-RGD may be used to assess the inhibition of the $\alpha_v\beta_3$ integrin by antagonists, a process by which optimization of the dose of $\alpha_v\beta_3$ antagonists may be achieved. Finally, $\alpha_v\beta_3$ expression has been reported to be an important factor in determining the invasiveness and metastatic potential of malignant tumors in experimental tumor models as well as in patient studies (20, 21). Therefore, noninvasive imaging of $\alpha_v\beta_3$ expression using [^{18}F]Galacto-RGD and PET may provide a unique means of characterizing the biological aggressiveness of a malignant tumor in an individual patient.

In conclusion, our study demonstrates that [^{18}F]Galacto-RGD is suitable for imaging of $\alpha_v\beta_3$ expression using PET. Moreover, we have shown that this tracer, in combination with a small animal PET scanner, may be used to monitor the blockade of $\alpha_v\beta_3$ by specific antagonists in living mice. We anticipate that noninvasive serial studies of $\alpha_v\beta_3$ expression and functional activity using PET will become an important tool to evaluate the role of $\alpha_v\beta_3$ during tumor progression and angiogenesis in basic research as well as in clinical studies.

Acknowledgments

The RDS-cyclotron team, particularly M. Herz, is acknowledged for routine radionuclide production. We thank W. Linke, S. Daum, F. Rau, and K. Fischer for excellent technical assistance and B. J. Pichler, G. Boening, and M. Rafecas for their contribution in preparing the PET images. We thank Dr. D. A. Cheresh for supplying us with M21 and M21-L melanoma cells.

References

1. Clezardin, P. Recent insights into the role of integrins in cancer metastasis. Cell. Mol. Life Sci., *54:* 541–548, 1998.
2. Stromblad, S., and Cheresh, D. A. Integrins, angiogenesis and vascular cell survival. Chem. Biol., *3:* 881–885, 1996.
3. Gurrath, M., Müller, G., Kessler, H., Aumailley, M., and Timpl, R. Conformation/activity studies of rationally designed potent anti-adhesive RGD peptides. Eur. J. Biochem., *210:* 911–921, 1992.
4. Haubner, R., Finsinger, D., and Kessler, H. Stereoisomeric peptide libraries and peptidomimetics for designing selective inhibitors of the $\alpha_v\beta_3$ integrin for a new cancer therapy. Angew. Chem. Int. Ed. Engl., *36:* 1374–1389, 1997.
5. Aumailley, M., Gurrath, M., Müller, G., Calvete, J., Timpl, R., and Kessler, H. Arg-Gly-Asp constrained within cyclic pentapeptides. Strong and selective inhibitors of cell adhesion to vitronectin and laminin fragment P1. FEBS Lett., *291:* 50–54, 1991.

6. Carron, C. P., Meyer, D. M., Pegg, J. A., Engleman, V. W., Nickols, M. A., Settle, S. L., Westlin, W. F., and Ruminski, P. G., and Nickols, G. A. A peptidomimetic antagonist of the integrin $\alpha_v\beta_3$ inhibits Leydig cell tumor growth and the development of hypercalcemia of malignancy. Cancer Res., *58:* 1930–1935, 1998.
7. Kerr, J. S., Wexler, R. S., Mousa, S. A., Robinson, C. S., Wexler, E. J., Mohamed, S., Voss, M. E., Devenny, J. J., Czerniak, P. M., Gudzelak, A., Jr., and Slee, A. M. Novel small molecule α_v integrin antagonists: comparative anti-cancer efficacy with known angiogenesis inhibitors. Anticancer Res., *19:* 959–968, 1999.
8. Lode, H. N., Moehler, T., Xiang, R., Jonczyk, A., Gillies, S. D., Cheresh, D. A., and Reisfeld, R. A. Synergy between an antiangiogenic integrin α_v antagonist and an antibody-cytokine fusion protein eradicates spontaneous tumor metastases. Proc. Natl. Acad. Sci. USA, *96:* 1591–1596, 1999.
9. Sipkins, D. A., Cheresh, D. A., Kazemi, M. R., Nevin, L. M., Bednarski, M. D., and Li, K. C. P. Detection of tumor angiogenesis *in vivo* by $\alpha_v\beta_3$-targeted magnetic resonance imaging. Nat. Med., *5:* 623–626, 1998.
10. Wester, H. J., Hamacher, K., and Stöcklin, G. A comparative study of n.c.a. fluorine-18 labeling of proteins via acylation and photochemical conjugation. Nucl. Med. Biol., *23:* 365–372, 1996.
11. Haubner, R., Wester, H. J., Reuning, U., Senekowitsch-Schmidtke, R., Diefenbach, B., Kessler, H., Stöcklin, G., and Schwaiger, M. Radiolabeled $\alpha_v\beta_3$ integrin antagonists: a new class of tracers for tumor targeting. J. Nucl. Med., *40:* 1061–1071, 1999.
12. Cheresh, D. A., and Spiro, R. C. Biosynthetic and functional properties of an Arg-Gly-Asp-directed receptor involved in human melanoma cell attachment to vitronectin, fibrinogen, and von Willebrand factor. J. Biol. Chem., *262:* 17703–17711, 1987.
13. Ziegler, S. I., Pichler, B. J., Boening, G., Rafecas, M., Pimpl, W., Lorenz, E., Schmitz, N., and Schwaiger, M. A prototype high resolution animal positron tomograph with avalanche photodiode arrays and LSO crystals. Eur. J. Nucl. Med., *28:* 136–143, 2001.
14. Haubner, R., Gratias, R., Diefenbach, B., Goodman, S. L., Jonczyk, A., and Kessler, H. Structural and functional aspects of RGD-containing cyclic pentapeptides as highly potent and selective integrin $\alpha_v\beta_3$ antagonists. J. Am. Chem. Soc., *118:* 7461–7472, 1996.
15. Sivolapenko, G. B., Skarlos, D., Pectasides, D., Stathopoulou, E., Milonakis, A., Sirmalis, G., Stuttle, A., Courtenay-Luck, N. S., Konstantinides, K., and Epenetos, A. A. Imaging of metastatic melanoma utilising a technetium-99m-labelled RGD-containing synthetic peptide. Eur. J. Nucl. Med., *25:* 1383–1389, 1998.
16. De Jong, M., Van Hagen, P. M., Breeman, W. A., Bernard, H. F., Schaar, M., Van Gameren, A., Srinivasan, A., Schmidt, M., Bugaj, J. E., and Krenning, E. P. Evaluation of a radiolabeled cyclic DTPA-RGD analog for tumor imaging and radionuclide therapy. J. Nucl. Med., *41:* 232P, 2000.
17. Janssen, M. L. H., Boerman, O. C., Edwards, D. S., Barnett, J. A., Rajopadhye, W. J., Oyen, G., and Corstens, F. H. M. ^{111}In- and ^{99m}Tc-labeled peptides against the $\alpha_v\beta_3$ integrin: a new target for radionuclide peptide targeting of tumors. J. Nucl. Med., *41:* 33P, 2000.
18. Bock, M., Bruchertseifer, F., Haubner, R., Senekowitsch-Schmidtke, R., Kessler, H., Schwaiger, M., and Wester, H. J. Tc-99m-, Re-188- and Y-90-labeled $\alpha_v\beta_3$ antagonists: promising tracer for tumor-induced angiogenesis. J. Nucl. Med., *41:* 41P, 2000.
19. Brower, V. Tumor angiogenesis-new drugs on the block. Nat. Biotechnol., *17:* 963–968, 1999.
20. Felding-Habermann, B., Mueller, B. M., Romerdahl, C. A., and Cheresh, D. A. Involvement of integrin α_v gene expression in human melanoma tumorigenicity. J. Clin. Investig., *89:* 2018–2022, 1992.
21. Gasparini, G., Brooks, P. C., Biganzoli, E., Vermeulen, P. B., Bonoldi, E., Dirix, L. Y., Ranieri, G., Miceli, R., and Cheresh, D. A. Vascular integrin $\alpha_v\beta_3$: a new prognostic indicator in breast cancer. Clin. Cancer Res., *4:* 2625–2634, 1998.

Cancer Research
The Journal of Cancer Research (1916–1930) | The American Journal of Cancer (1931–1940)

AACR American Association for Cancer Research

Noninvasive Imaging of $\alpha_v\beta_3$ Integrin Expression Using ^{18}F-labeled RGD-containing Glycopeptide and Positron Emission Tomography

Roland Haubner, Hans-Jürgen Wester, Wolfgang A. Weber, et al.

Cancer Res 2001;61:1781-1785.